Imaging scarred states in quantum dots

2009 J. Phys.: Condens. Matter 21 212201

(http://iopscience.iop.org/0953-8984/21/21/212201)

IOP FTC
IOP PUBLISHING JOURNAL OF PHYSICS: CONDENSED MATTER
J. Phys.: Condens. Matter **21** (2009) 212201 (5pp) doi:10.1088/0953-8984/21/21/212201

FAST TRACK COMMUNICATION

Imaging scarred states in quantum dots

A M Burke[1], R Akis[1], T Day[1], G Speyer[1], D K Ferry[1,2] and B R Bennett[3]

[1] Department of Electrical Engineering and Center for Solid State Electronics Research, Arizona State University, Tempe, AZ 85287-5706, USA
[2] Department of Physics, Arizona State University, Tempe, AZ 85287-5706, USA
[3] Naval Research Laboratory, Washington, DC 20375, USA

Received 2 April 2009, in final form 6 April 2009
Published 24 April 2009
Online at stacks.iop.org/JPhysCM/21/212201

Abstract
We have used the scanning gate microscopy technique to image scar structures in an open quantum dot, fabricated in an InAs quantum well and defined by electron beam lithography. These are shown to have a periodicity in magnetic field that correlates with that found in the conductance fluctuations. Simulations have shown that these magnetic transform images bear a strong resemblance to actual scars found in the dots.

(Some figures in this article are in colour only in the electronic version)

1. Introduction

The measurement of open quantum systems has been of general interest since the beginnings of quantum mechanics [1]. This is a basic ingredient of quantum information processing, which has become of interest in connection with quantum computing [2]. Mesoscopic quantum dots have been a particular example in which quantum interference plays a significant role in the measured transport properties [3]. Open quantum dots offer unique information as they correspond to a mixed classical phase space [4] wherein some of the quantum states couple to the outside environment through the dot's confining constrictions and are therefore heavily decohered. Other states within the cavity, known as pointer states, remain robust as they do not couple out of the dot [5, 6]. Previously these states could only be investigated using external measurements [7, 8]. However, the recent advent of scanning gate microscopy (SGM) [9] has allowed the probing of quantum structures within constrictions by rastering a biased AFM tip over the area of interest while concurrently mapping the resulting variations in conductance. This technique has been applied to investigate the quantum Hall edge states and localized regions of quantum point contacts (QPC) [10–12] as well as the classical and quantum behaviors within quantum dots in a GaAs/AlGaAs heterojunction material [13, 14].

Previous attempts to image the scarring functions have not yielded clear images, perhaps due to the larger effective mass of GaAs, more disorder in the samples, higher perturbation level used or larger dot size [13, 14]. Here, we present what we believe to be definitive measurement of pointer state scars in a quantum dot in InAs. The use of InAs, with its higher g-factor, and therefore more pronounced response to magnetic field, is coupled to a smaller dot geometry and lower perturbation applied from the tip. We discuss the images of two different scarring states which are periodic in magnetic field as expected from earlier considerations [15], and discuss their connection with expected quantum structures in these open quantum dots.

2. Experimental details

In figure 1, an AFM image of the sample is shown. The device was grown on a semi-insulating GaAs substrate. The heterostructure consists of a 1.5 μm strain relaxed $Al_{0.7}Ga_{0.3}Sb$ layer, a 12 nm thick InAs quantum well transport layer, an $In_{0.2}Al_{0.8}Sb$ confinement layer in which Tellurium was used as a delta dopant, and a 2 nm InAs cap layer used to passivate the wafer. Electron beam lithography (EBL) was used to write the quantum dot pattern, which designates the dot area as well as defining the dot openings via in-plane etched quantum point contacts (QPC). The in-plane QPCs are used to avoid having surface metal which will interfere with the scanning gate tip [10–12, 14]. The dot was designed to be 1.1 μm × 1.1 μm inner dimensions and the QPCs on either side have 600 nm openings and 100 nm lengths. The dot resides in a Hall bar sample and contact to the InAs transport layer is made along

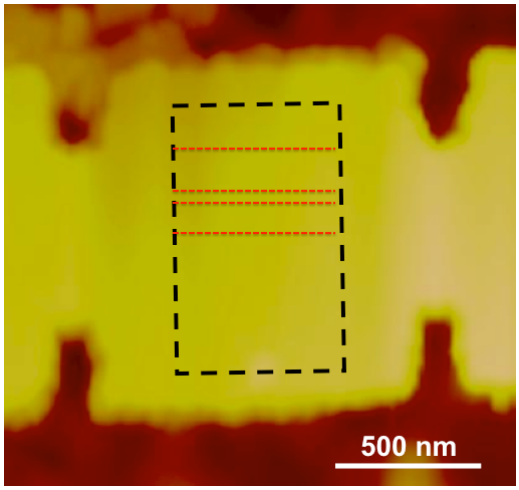

Figure 1. AFM scan of the dot. Inner dimensions measure 1.1 μm × 1.1 μm. QPC openings are 600 nm. The dashed line outlining a box indicates the SGM scan area, which is 864 nm vertically and 576 nm horizontally. The four dotted lines indicate the approximate positions of row scans discussed later.

the perimeter of the Hall bar contact arms where the metal coats the sidewall. The completed sample was then pasted to the SGM sample stage and bonded using a Au ball bonder. To insulate the sample from the SGM tip a thin layer of PMMA is spun onto the sample, and baked before the sample is loaded into the system. The total distance from the PMMA surface to the transport layer is 40 nm.

The sample is then mounted in a He3 cryostat and scanned with an Omicron low temperature AFM, in which the latter tip is metalized using PtIr so that a negative DC bias can be applied to create the perturbation. The entire cryostat is isolated on three Minus K vibration isolation tables. Magnetic fields perpendicular to the electron flow in the sample are provided by a super-conducting magnet in the dewar capable of continuous fields up to ±8 T. All measurements are carried out at 280 mK using lock-in amplifier bias and measurement under constant current conditions, and sample conductance is monitored in a four terminal configuration. From Shubnikov–de Haas measurements, the density is 1.5×10^{12} cm^{-2} and the mobility is estimated to be 65 000 cm^2 V^{-1} s^{-1} from another sample from the same wafer.

SGM uses the biased tip to raster, at a constant lift height above the sample surface, and acts as a local perturbation. The bias from the tip lifts the local Fermi energy, thus depleting the electron density beneath the tip. As the tip comes to areas of high electron density, it produces a large effect on the conductance. In contrast, in areas of low electron density, low change in conductance is recorded. At each point, as the tip is rastered, this change in the conductance through the device, as a result of the perturbation at that point, is measured and recorded. From this, a two-dimensional image of the change in conductance is generated. Figure 1 has an overlay defining the range over which the SGM image is formed. This area lies entirely within the quantum dot, and defines a scan area of 864 × 576 nm^2. Images are formed using a lift height of 100 nm from the PMMA surface and a tip bias of −0.4 V. The tip lift and bias conditions resulted in a small perturbation, causing changes in conductance below $0.2G_o$ ($G_o = 2e^2/h$) throughout the scan.

3. Results and discussion

It has been found that the existence of pointer states leads to quasi-periodic magnetoconductance oscillations that exhibit Fano line shapes [16]. These appear at magnetic fields below that for which a cyclotron orbit can fit entirely within the dot. This requirement ensures that the trajectory of an electron flowing through the device must come into contact with the hard walls of the dot and resonate within the dot before finally coupling to one of the leads. In figure 2(a), we plot the magnetoconductance of the dot in the range ±0.3 T, the lower limit of magnetic field for which the foregoing constraint holds. The background is removed from this magnetoconductance,

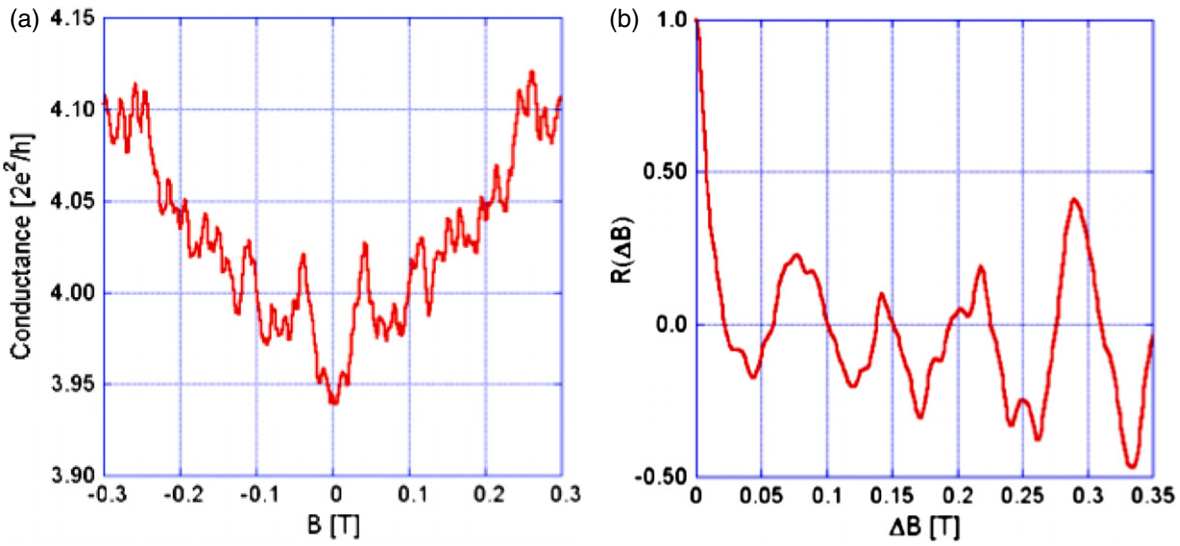

Figure 2. (a) Magnetoconductance through the dot from −300 to 300 mT. (b) Auto correlation of the magnetoconductance shown in (a).

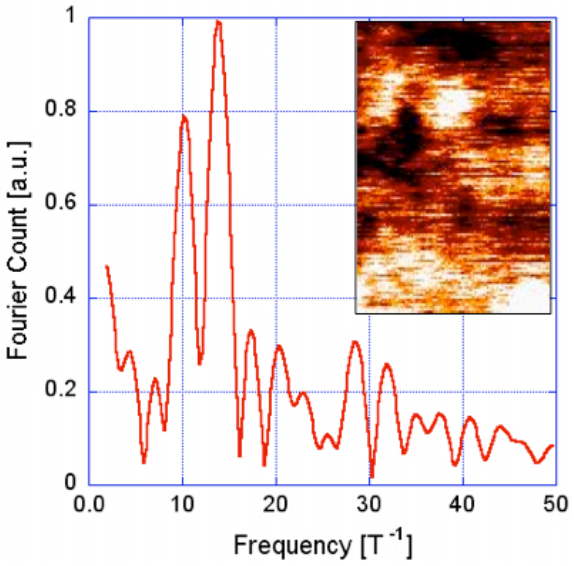

Figure 3. Fourier transform of the autocorrelation shown in figure 2(b). Inset: a typical scan, at 200 mT, with the background masking features. The scan size is 864 nm vertically and 576 nm horizontally.

and the autocorrelation function, in magnetic field, of the fluctuations is performed, as shown in figure 2(b). Here, there are repetitive oscillations, rather than a single simple decay, and this is indicative of the correlated behavior of recurring scars [17]. The Fourier transform of the autocorrelation function is shown in figure 3. There are two major peaks, at $10.6T^{-1}$ and $13.6T^{-1}$, which are thought to be indicative of the major recurring scars [7].

A family of images for varying magnetic field up to 300 mT was taken. These images were taken every 10 mT. Each image is a result of 120 raster scans (which are horizontal rows, discussed below) across the image area, designated in figure 1. By comparing signals between line scans, we estimate that the SGM resolution is in the 5–10 nm range. A typical scan, at 200 mT, is shown as the inset to figure 3. Features within the scan are masked by the background. To try to remove this masking the 0 T scan image was subtracted from each of the other images to show features that are functions of both the biased tip perturbation as well as change in magnetic field. A clear evolution of patterns then begins to appear in the images. From these, we highlight two such patterns which correlate with the magnetic frequencies in the autocorrelation function. In figure 4(a), two images of the raster line scans as a function of magnetic field are shown. Here, the rows indicate which of the 120 row scans is used, and the position is approximately indicated in figure 1. It is clear that a periodic structure in magnetic field is beginning to be observable. Structures which appear to be periodic in magnetic field are circled for ease of identification. The particular feature in (a) appears to have a period near $10T^{-1}$. Similarly, in figure 4(b), two images of the raster line scans as a function of magnetic field are shown, which appear to have a periodic structure near $13.6T^{-1}$.

As a consequence of the observations in figure 4, the Fourier transform, with respect to magnetic field, was performed for the entire set of images. Since the magnetoconductance through the sample was symmetric in B as seen in figure 2(a), a cosine transform was used, since the sine component of the Fourier transform would cancel out in summation. The cosine function incorporates a phase shift appropriate to magnetic fields which exhibited peaks in the row analysis. The equation for the transform becomes:

$$F(\omega) = \int I(B)\cos(\omega B + \varphi)\mathrm{d}B,$$

where $I(B)$ is the image at each magnetic field, ω is the frequency $(2\pi f)$ where f is the magnetic frequency, and φ is the shift in phase to align the function to a known peak in B. The frequency and the relative phase shift were adjusted to find the best response, although the range of magnetic frequencies was focused upon the peaks occurring in figure 3. From this, it was found that there was a single resulting magnetic frequency that gave a higher overall meaningful picture of the periodic scar structure. These images occurred at frequencies of 9.6 and $13.6T^{-1}$, in strong correlation to the peaks exhibited in figures 3 and 4.

It was found that one strong scar in the transform occurred at a magnetic frequency of $9.6T^{-1}$, and this image is shown in figure 5(a). To compare with this, we have performed simulations of the actual quantum dot, using a iterative solution to the Lippmann–Schwinger equation [18]. As the simulations are done at 0 K, the magnetoconductance trace was smoothed, and a Fourier transform indicated a dominant peak near that found in experiment. In addition, the dot simulated was made slightly asymmetric to gain better agreement with the experiment. In figure 5(b), we plot one of the scars found in this simulation. This scar occurs near a magnetic field for which figure 4(a) has a peak. While there is not an exact match, the image in figure 5(a) clearly seems to form part of the diamond structure found in the simulation. It is difficult to exactly align the experimental structure with the theoretical one, it seems to be the case that the diamond like structure in the bottom of figure 5(a) corresponds to the diamond like scar in the bottom of figure 5(b). In a symmetric dot, the diamond shape would be fully replicated in the upper half. This type of state is usually found with a vortex state embedded within the diamond [19, 20], in which the vortex is defined by the line integral of momentum around a closed contour (here a circle). Classically, this integral vanishes, but it is quantized in units of nh quantum mechanically [20]. Hence, this circulating current creates a quantized magnetic dipole which interacts self-consistently with the dot. It is not clear here, whether the image in figure 5(a) is of the scar or the enclosed vortex state.

A second magnetic periodicity and image was found at $13.6T^{-1}$, and this image is shown in figure 6(a). It is clear that this image is quite different from that in figure 5(a). In figure 6(b), we plot a recurring scar that is found near a peak shown in figure 4(b), and bearing a strong resemblance to the image. The agreement seems to be fairly good, but we find in the simulation that disorder strongly disrupts these images. In addition, we find by simulating the scanning tip, that the tip bias can also distort the images, as presumed above. Hence, it is quite exciting to find scars that bear strong resemblance to the actual data produced from the experiment.

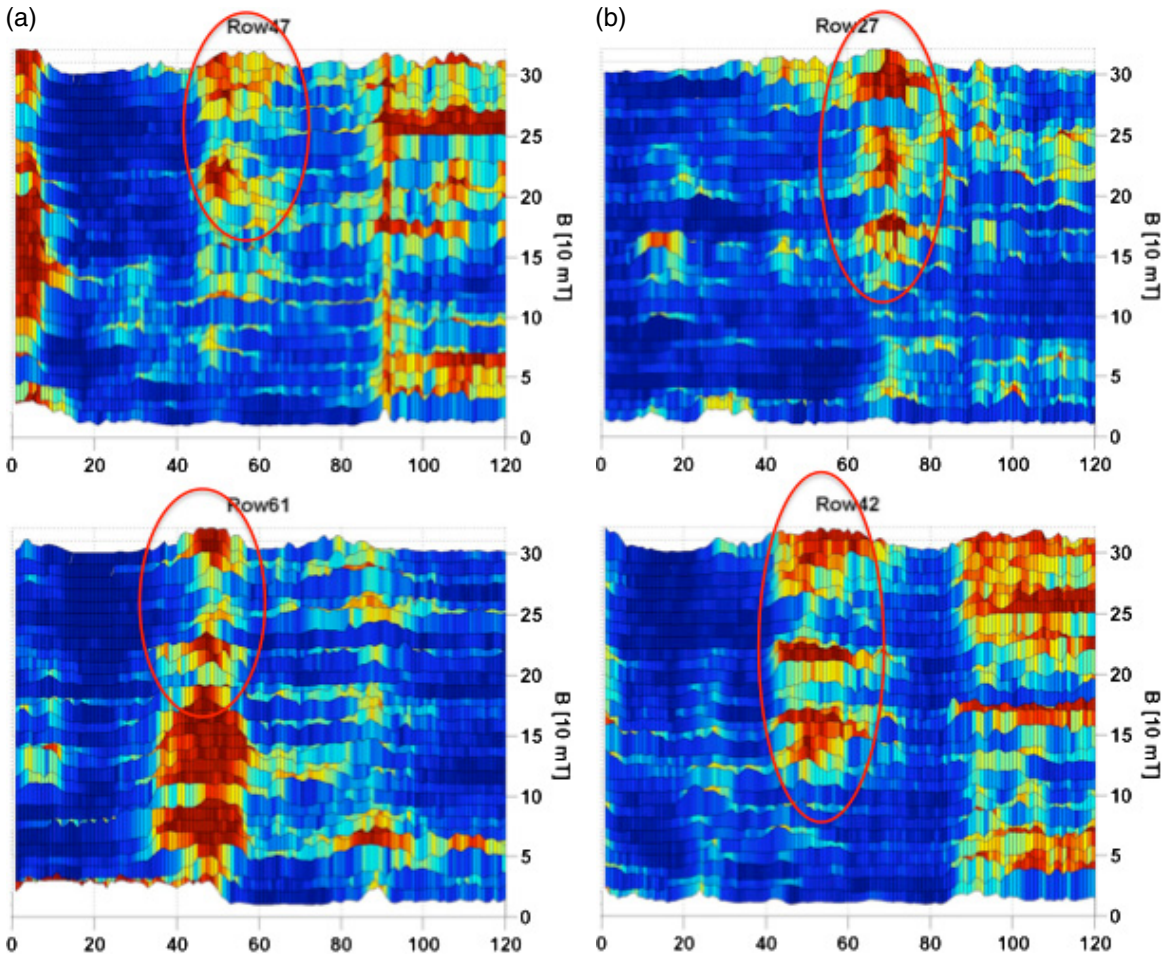

Figure 4. Raster line scans (horizontal) as a function of magnetic field (vertical). The row is designated above the image and refers to one of the line scans in figure 1. (a) Two rows where feature appears to have a periodicity near $10T^{-1}$. (b) Two rows which have a periodicity near $13.6T^{-1}$. Structures which appear to be periodic in magnetic field are circled for ease of observation.

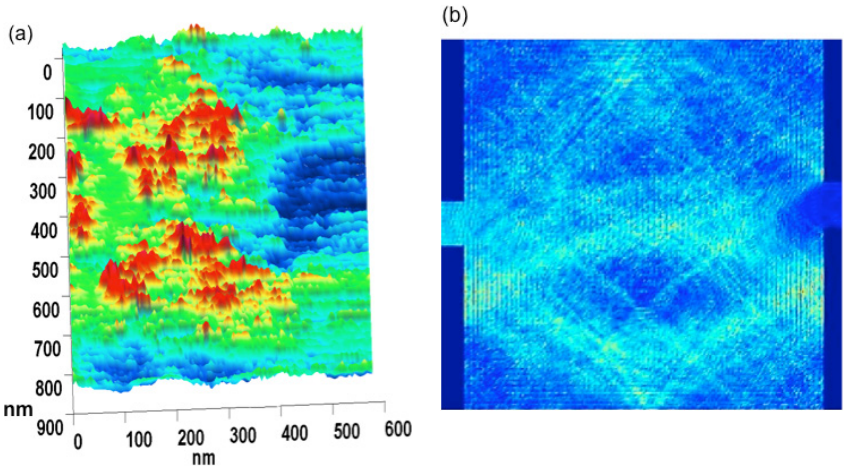

Figure 5. (a) Fourier transform of the images with respect to magnetic field, showing structure with a periodicity of $9.6T^{-1}$. (b) Simulation of the scar state which occurs near a magnetic field for which the image has a peak that contributes to the transform in (a). The vertical axes and color coding on the figures are arbitrary units.

An interesting aspect of the use of the Fourier transform in magnetic field is the connotation this has for quantum physics. The magnetic field generally produces a diamagnetic shift of the energies which pushes states upward through the Fermi level, thus depopulating them. The fact that the scar recurs in an entire set of states, for the same bias conditions, suggests that this scar state is imprinted in an entire family of propagating states of the dot, or that the robust state at the

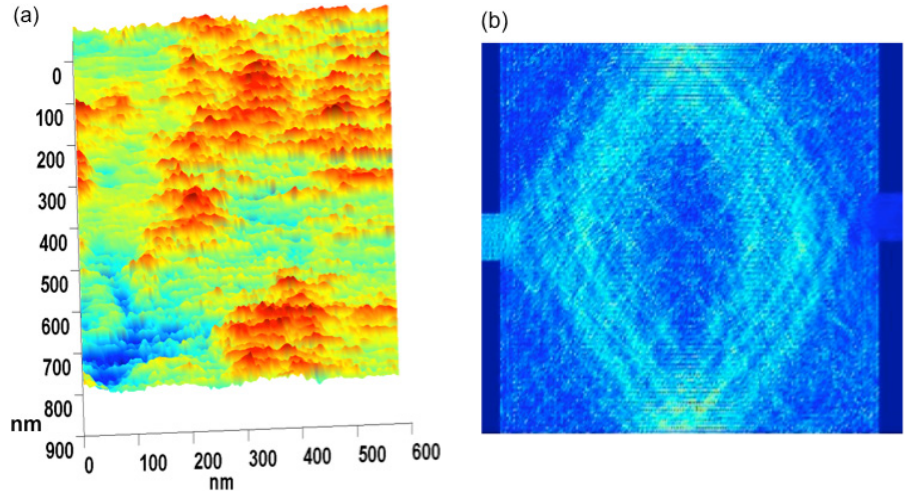

Figure 6. (a) Image from the Fourier transform at $13.6T^{-1}$. The image is less distinct that than figure 5(a), but the key features can be discerned. (b) Recurring scar found in the simulation that bears a strong resemblance to the experimental image. The vertical axes and color coding on the figures are arbitrary units.

Fermi level has an entire set of daughter states within the other occupied states of the dot. We have previously connected this behavior to the concept of quantum Darwinism [21], so that this work can also give new insight into this phenomenon by observing its effect in an experimental system.

In summary, we have used SGM techniques to image scar structures in an open quantum dot and have shown that these have a periodicity in magnetic field that correlates to that found in the conductance fluctuations. We should remark that these scars are similar in nature to those found in classical microwave cavity experiments [22], at least within the current understanding of the decoherence theory of quantum physics. Simulations have shown that these magnetic transform images bear a strong resemblance to actual scars found in the dots.

Acknowledgments

This work was supported in part by the Office of Naval Research and a grant from Arizona State University's GPSA Graduate Research Support Program. AMB is supported by an Applied Materials doctoral fellowship. The authors would like to extend special thanks to G M Jones and J B Boos for technical discussions regarding material processing, N Aoki for discussions related to SGM measurements, and to C Tracy, L Cooper, and S M Goodnick for helpful discussions throughout this study in its entirety.

References

[1] Schrödinger E 1935 *Naturwissenschaften* **23** 807
Schrödinger E 1935 *Naturwissenschaften* **23** 844
[2] DiVincenzo D P 1995 *Science* **270** 255
[3] Bird J P, Akis R, Ferry D K, de Moura A P S, Lai Y-C and Indlekofer K M 2003 *Rep. Prog. Phys.* **66** 583
[4] Ketzmerick R 1996 *Phys. Rev.* B **54** 10841
[5] Zurek W H 2003 *Rev. Mod. Phys.* **75** 715
[6] Ferry D K, Akis R and Bird J P 2004 *Phys. Rev. Lett.* **93** 026803
[7] Bird J P, Akis R, Ferry D K, Vasileska D, Cooper J, Aoyagi Y and Sugano T 1999 *Phys. Rev. Lett.* **82** 4691
[8] De Moura A P S, Lai Y-C, Akis R, Bird J P and Ferry D K 2002 *Phys. Rev. Lett.* **88** 236804
[9] Topinka M A, LeRoy B J, Heller S E J, Westervelt R M, Maranowski K D and Gossard A C 2000 *Science* **289** 2323
LeRoy B J 2003 *J. Phys.: Condens. Matter* **15** R1835
Aidala K E, Parrott R E, Kramer T, Heller E J, Westervelt R M, Hanson M P and Gossard A C 2007 *Nat. Phys.* **3** 464
[10] Crook R, Smith C G, Barnes D H W, Simmons M Y and Ritchie D A 2000 *J. Phys.: Condens. Matter* **12** L167
Crook R, Smith C G, Simmons M Y and Ritchie D A 2000 *J. Phys.: Condens. Matter* **12** L735
Crook R, Smith C G, Simmons M Y and Ritchie D A 2001 *J. Phys.: Condens. Matter* **13** L249
Aoki N, da Cunha C R, Akis R, Ferry D K and Ochiai Y 2005 *Appl. Phys. Lett.* **87** 223501
Pioda A, Kičin S, Brunner D, Ihn T, Sigrist M, Ensslin K, Reinwald M and Wegscheider W 2007 *Phys. Rev.* B **75** 045433
[11] Aoki N, da Cunha C R, Akis R, Ferry D K and Ochiai Y 2005 *Phys. Rev.* B **72** 155327
[12] da Cunha C R, Aoki N, Morimoto T, Ochiai Y, Akis R and Ferry D K 2006 *Appl. Phys. Lett.* **89** 242109
[13] Crook R, Smith C G, Graham A C, Farrer I, Beere H E and Ritchie D A 2003 *Phys. Rev. Lett.* **91** 246803
[14] Burke A M, Aoki N, Akis R, Ochiai Y and Ferry D K 2008 *J. Vac. Sci. Technol.* B **26** 1488
[15] Ferry D K, Akis R and Bird J P 2005 *J. Phys.: Condens. Matter* **17** S1017
[16] Akis R, Bird J P and Ferry D K 2002 *Appl. Phys. Lett.* **81** 129
[17] Akis R, Bird J P, Vasileska D, Ferry D K, de Moura A P S and Lai Y-C 2003 *Electron Transport in Quantum Dots* ed J P Bird (Boston, MA: Kluwer Academic) p 209
[18] Akis R, Ferry D K and Bird J P 1996 *Phys. Rev.* B **54** 17705
[19] Barker J R, Akis R and Ferry D K 2000 *Superlatt. Microstruc.* **27** 319
[20] Barker J R 2003 *Progress in Nonequilibrium Green's Functions II* ed M Bonitz and D Semkat (Singapore: World Scientific) p 198
[21] Brunner R, Akis R, Ferry D K, Kuchar F and Meisels R 2008 *Phys. Rev. Lett.* **101** 024102
[22] Kim Y H, Barth M, Kuhl U, Stöckmann H-J and Bird J P 2003 *Phys. Rev.* B **68** 045315